NANO LETTERS

pubs.acs.org/NanoLett Letter

Thermally Assisted Rashba Splitting and Circular Photogalvanic Effect in Aqueously Synthesized 2D Dion–Jacobson Perovskite Crystals

Boxuan Zhou,[#] Lihan Liang,[#] Jiaqi Ma, Junze Li, Wancai Li, Zeyi Liu, Haolin Li, Rui Chen, and Dehui Li*

Cite This: *Nano Lett.* 2021, 21, 4584–4591 Read Online

ACCESS | Metrics & More | Article Recommendations | Supporting Information

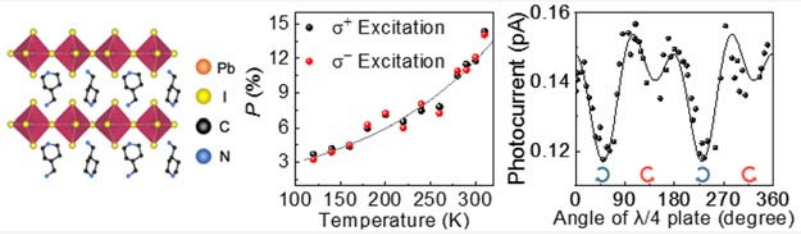

ABSTRACT: Recently, a two-dimensional Dion–Jacobson (DJ) perovskite (AMP)PbI_4 (AMP = 4-(aminomethyl)piperidinium) is emerging with remarkable Rashba effect and ferroelectricity. However, the origin of the giant Rashba splitting remains elusive and the current synthetic strategy via slow cooling is time- and power-consuming, hindering its future applications. Here, we report on an economical aqueous method to obtain (AMP)PbI_4 crystals and clarify the origin of the giant Rashba effect by temperature- and polarization-dependent photoluminescence (PL) spectroscopy. The strong temperature-dependent PL helicity indicates the thermally assisted structural distortion as the main origin of the Rashba effect, suggesting that valley polarization still preserves at high temperatures. The Rashba effect was further confirmed by the circular photogalvanic effect near the indirect bandgap. Our study not only optimizes the synthetic strategies of this DJ perovskite but also sheds light on its potential applications in room/high-temperature spintronics and valleytronics.

KEYWORDS: *2D Dion-Jacobson perovskite, aqueous synthesis, Rashba effect, circular photogalvanic effect*

In materials with strong spin–orbit interaction and broken inversion symmetry, the spin-degenerate parabolic band will split into two spin-polarized bands, which is called the Rashba–Dresselhaus effect.[1] Conventionally, the Rashba and Dresselhaus effect are associated with surface-induced and bulk asymmetry, respectively, and we use the term "Rashba effect" to denote the "Rashba–Dresselhaus effect" hereafter for brevity. Materials with the Rashba effect have attracted growing attention due to their large spin-to-charge conversion efficiency[1,2] and thus find promising applications in spintronics.[3] For practical applications, a larger Rashba splitting benchmarked by Rashba splitting energy (E_R) is preferred to achieve efficient spin manipulation by electric field[1−6] or interface engineering[7] without requiring an external magnetic field.

Rashba effect has been extensively investigated in various material systems including III–V semiconductor heterostructures[5] and topological insulators Bi_2Se_3[6] over the past few decades. Nevertheless, Rashba splitting energy in these materials is typically smaller than 10 meV, limiting the performance of spintronic devices based on these materials.[2] Recently, a giant Rashba splitting energy of ∼110 meV has been observed in three-dimensional (3D) organic–inorganic halide perovskites (HOIP).[8] The remarkable splitting of 3D HOIP was found to arise from a dynamical and thermal-induced effect, revealed by different techniques including polarization- and temperature-dependent transient absorption (TA),[9] photoluminescence (PL),[10,29,30] and photoconductivity[8,23,24] spectroscopy. Nevertheless, the inherent ambient instability of 3D HOIP is a big challenge for them to be applied in practice.[11−13] To address the stability issue, two-dimensional (2D) versions of the HOIP are introduced.[14,15] 2D Ruddlesden–Popper (RP) phase HOIP $(C_6H_5C_2H_4NH_3)_2PbI_4$ (PEPI) exhibits the Rashba effect with a smaller splitting of (40 ± 5) meV but with improved stability compared with 3D HOIP.[16] Very recently, a Rashba splitting of more than 80 meV was observed in an emergent

Received: January 27, 2021
Revised: May 18, 2021
Published: May 26, 2021

2D Dion–Jacobson (DJ) phase HOIP $(AMP)PbI_4$[17] (AMP = 4-(aminomethyl)piperidinium). Compared with the RP phase PEPI, the Rashba splitting energy of $(AMP)PbI_4$ is doubled, and the ambient stability is also improved, since the inorganic layers are held together by hydrogen bonding rather than van der Waals force (Figure 1a), leading to a smaller interlayer distance and thus enhanced ambient stability.[18−20] In addition, robust ferroelectricity was reported in $(AMP)PbI_4$ with a high Curie temperature T_c = 352 K, rendering it great potential in spintronic devices with both logic and storage functionalities.[17,21] Those factors make $(AMP)PbI_4$ a powerful 2D HOIP for spintronics.

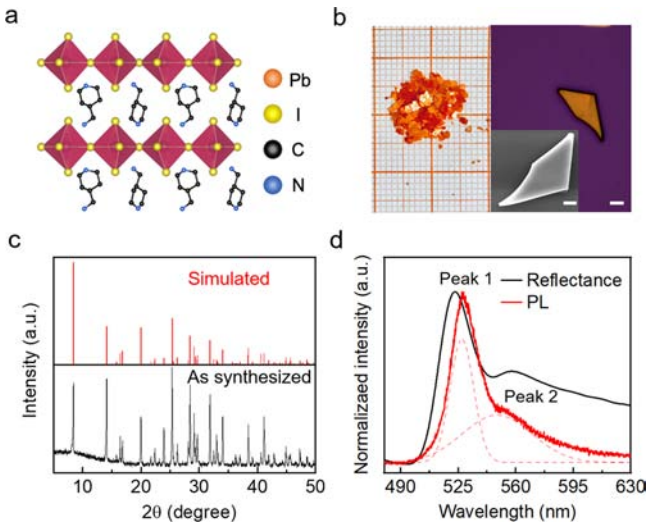

Figure 1. Crystal structure and characterizations of the aqueous synthesized $(AMP)PbI_4$. (a) Schematic illustration of crystal structures of $(AMP)PbI_4$. (b) Photograph of as-synthesized crystals (left) and the OM image of the exfoliated $(AMP)PbI_4$ microplate (right). Inset: the SEM image of the exfoliated sample. The scale bar is 10 μm. (c) Powder XRD patterns of $(AMP)PbI_4$: measured (bottom) and simulated (top) results. (d) PL and reflection spectra of as-synthesized $(AMP)PbI_4$. The red dashed lines are the fitting results using a Voigt function.

To fully explore the potentials of $(AMP)PbI_4$ in spintronics, it is essential to understand the origins of the large Rashba splitting. Nevertheless, experimental studies on the origin of the giant Rashba splitting in this type of 2D HOIPs are still missing up to date. In addition, currently $(AMP)PbI_4$ crystals are synthesized mainly by slow cooling,[17,19,22] which is very time- and power-consuming. To this end, it is urgent to develop an efficient synthetic strategy and reveal the underlying mechanism of the large Rashba splitting for further potential applications.

Here, we report on a highly economical and efficient aqueous method to synthesize $(AMP)PbI_4$ single crystals at room temperature. To identify the underlying mechanisms of the giant Rashba effect, we have conducted a series of temperature- and polarization-dependent PL studies. We found that the degree of the circularly polarized light emission increases with the temperature, suggesting that thermally assisted structural distortion might serve as the main origin of the Rashba effect, despite the static Rashba splitting caused by AMP cation induced inversion asymmetry is also present.[17] This was further supported by tracing the temperature-dependent characteristics of the indirect transition. The presence of the circular photogalvanic effect (CPGE)[8,23,24] also verifies the robust Rashba splitting of $(AMP)PbI_4$. In contrast to monolayer transition metal dichalcogenides (TMDs) where the degree of the circular polarization of steady-state PL typically vanishes at room temperature due to enhanced valley-depolarization processes,[25,26] the valley polarization of $(AMP)PbI_4$ is well preserved at high temperatures. The robust preservation of valley identity is important in valleytronic devices that require the control of charge carriers in different valleys.[25] We believe that our study is of great importance in understanding the electronic and structure relationship of $(AMP)PbI_4$, highlighting its potentials in room/high-temperature spintronic and valleytronic applications.

RESULTS AND DISCUSSION

Figure 1a displays the schematics of the crystal structure of $(AMP)PbI_4$, where each layer of $[PbI_6]^{4-}$ octahedra is sandwiched by one layer of AMP cations.[22] The single crystals

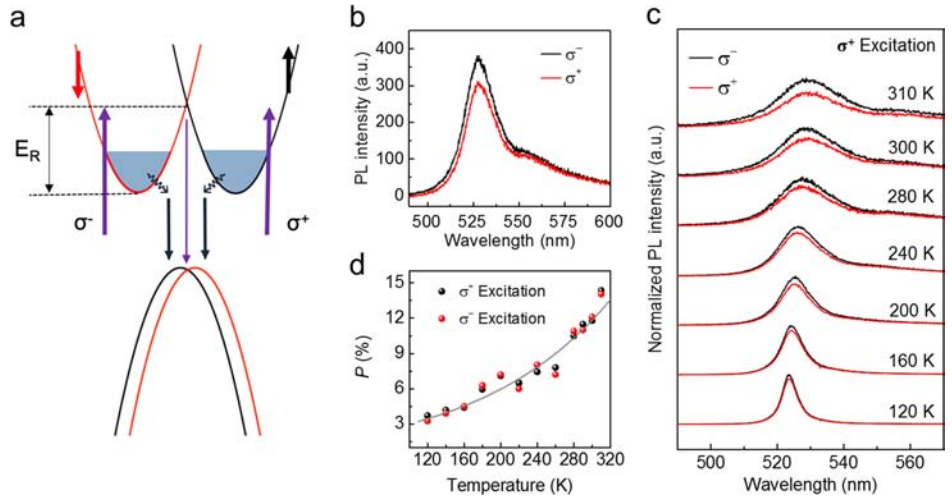

Figure 2. Circular polarization resolved PL measurement under circularly polarized light excitation. (a) Schematic illustration of the Rashba spin splitting bands and selective excitation with circularly polarized light. (b,c) Left and right circularly polarized PL spectra under right circularly polarized excitation at room temperature (b) and different temperatures (c). (d) Degree of circular polarization as a function of temperature.

https://doi.org/10.1021/acs.nanolett.1c00364
Nano Lett. 2021, 21, 4584−4591

were synthesized in deionized (DI) water at room temperature without external heating (Figure S1), similar to the previous report.[27] First, lead iodide (PbI_2) was dissolved in DI water after adding a certain amount of aqueous hydriodic acid (HI). Then, a mixture of aqueous CH_3NH_2 (MA) and AMP was carefully dropped into the resultant solution. Since the alkaline MA/AMP mixture was injected into the resultant acid solution, the neutralizing reaction will take place and spontaneously release heat. Afterward, the aqueous solution was left to stand still and the perovskites will crystallize in a few hours. It should be noted that the synthesis was conducted at room temperature, and thus this synthetic method is rather simple and efficient.

The as-synthesized crystals (left panel in Figure 1b) exhibit orange color with a lateral size of several millimeters. The optical microscopy (OM) image (right panel in Figure 1b) and scanning electron microscopy (SEM) image (inset in Figure 1b) of the exfoliated (AMP)PbI_4 suggest that the surface is smooth due to the 2D layered nature. The powder X-ray diffraction (PXRD) pattern of the as-synthesized crystals (Figure 1c) exhibits sharp peaks, consistent with simulation results based on the single crystal X-ray data.[17] Moreover, PL spectra show no noticeable change after being stored in ambience for a year (Figure S2), revealing the excellent long-term stability. Both the room-temperature PL and reflection spectra present two peaks (Figure 1d), which can be well fitted by using a Voigt function. It should be noted that bulk crystals are used for the reflection measurement in Figure 1d, whose thickness is orders of magnitude larger than the wavelength of incident light. Thus, the broad reflection peaks are unlikely to originate from Fabry−Perot resonance of the natural quantum well material. While the high energy peak (peak 1) located around 529 nm can be attributed to free excitons, we ascribe the lower energy emission peak (peak 2) in the sub-bandgap regime to the indirect bandgap transition due to the Rashba splitting,[28−30] which we will illustrate in detail later.

Figure 2a gives the band structure with Rashba splitting which is composed of two branches with opposite spin orientations. The conduction band possesses a much larger splitting in perovskites due to its stronger Pb p orbital character that contributes to the spin−orbit coupling (SOC).[8] As illustrated in Figure 2a, circularly polarized light pumping can selectively excite carriers with specific spin orientations, resulting in the helicity of PL emission due to optical selection rules.[17,29,30,38] On this basis, we have conducted circular polarization-resolved PL studies to verify the Rashba effect. In our experiment, a circularly polarized 473 nm laser was used to excite the sample, and PL emission was analyzed by a polarization-resolved detection system (the experimental setup is shown in Figure S3). Figure 2b shows the left (σ^-) and right (σ^+) circularly polarized PL upon σ^+ polarized light excitation at room temperature. The peak intensity difference between different circularly polarized components is clearly observed, suggesting the presence of Rashba splitting in our (AMP)PbI_4 crystals. Quantitatively, the degree of circular polarization of PL (P) is defined as[39]

$$P = \left| \frac{I(\sigma^+) - I(\sigma^-)}{I(\sigma^+) + I(\sigma^-)} \right| \quad (1)$$

where $I(\sigma^+)$ and $I(\sigma^-)$ represent the maximum σ^+ and σ^- polarized PL intensity under the same circularly polarized light excitation. We have measured 12 samples, and the average P is estimated to be 13% at room temperature (the experimental error is illustrated in Figure S4 and the statistical histogram of P is shown in Figure S5). The relatively large variation of P might be attributed to the different thickness and surface morphology of different samples, which is common in the PL helicity measurements.[27,39,40] For the same sample, P remains unchanged when the excitation power changes in the range of our measurement (Figure S6). P increases significantly under near-resonant excitation (532 nm), while it drops to zero under 405 nm excitation (Figure S7). This is similar to the results reported in 3D perovskites,[30] suggesting that phonon-scattering in the hot carrier relaxation process might reduce the degree of PL helicity. Based on the measured P value, we further quantify Rashba splitting energy E_R to be ∼90 meV at room temperature through a model that correlates hot carrier cooling rate and spin-flip rate (see Supporting Information), similar to the previously reported value.[17]

Temperature-dependent PL helicity measurements under σ^+ and σ^- excitation were also carried out to study how P evolves with temperature. Since P is too small to be detectable at cryogenic temperature, we only plot circular-polarization-resolved PL spectra from 120 to 310 K as shown in Figure 2c (PL spectra under σ^- excitation and additional temperature points are shown in Figure S8). In the temperature range of measurements, phase transition can be excluded by the temperature-dependent PXRD patterns (Figure S9). To clearly see the temperature-dependent trend, we extracted P values and plotted against temperature in Figure 2d. At each temperature point, the P values are very close under excitation of different handiness, indicating that such circularly polarized light emission is an intrinsic property. Interestingly, the P value increases slowly in the low-temperature regime and faster at higher temperatures. This peculiar phenomenon suggests that a thermally assisted Rashba effect might contribute to the overall splitting, despite the temperature-independent static Rashba effect arising from AMP cations induced non-centrosymmetry or surface/interface distortions.[17,38] By elevating the temperature, the thermally assisted Rashba splitting becomes prominent, leading to a rapid increase of P values. For typical valleytronic materials like TMDs, the P values will vanish at room temperature due to enhanced valley-depolarization processes.[25,26] The increased P value of (AMP)PbI_4 at room temperature suggests that the valley polarization can be well preserved at higher temperatures, which is of great importance for room-temperature or even high-temperature valleytronics. One possible reason is that the thermally assisted Rashba effect introduces a larger spin-splitting at higher temperatures, which can counteract the influence of depolarization processes. Although a larger exciton population is expected to occupy higher-energy states at high temperature which could lead to a small P value, the larger spin-splitting energy at higher temperatures introduced by the thermally assisted Rashba effect in our case dominates over the static Rashba effect, which finally determines the temperature evolution of P. As a result, we observed that P increases with the increase of temperature.

The Rashba effect can also introduce an indirect bandgap transition with lower transition energy due to the momentum-dependent band splitting (Figure 2a), as widely reported in halide perovskites.[28−30] At room temperature, the energy difference between peak 1 and 2 is 95 meV (Figure 1d), which coincides with the E_R (∼90 meV) estimated from room-temperature circularly polarized PL spectra. Thus, the low-

https://doi.org/10.1021/acs.nanolett.1c00364
Nano Lett. 2021, 21, 4584−4591

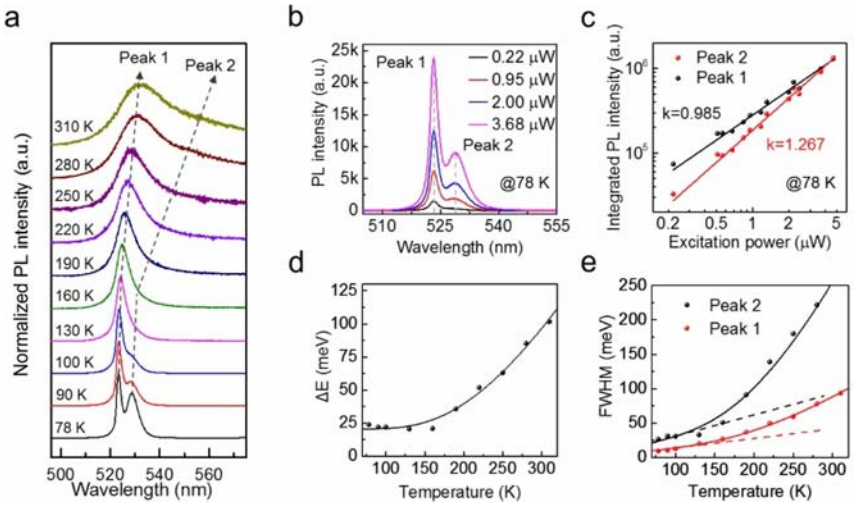

Figure 3. Temperature-dependent PL spectra upon linearly polarized light excitation. (a) Temperature-dependent PL spectra of $(AMP)PbI_4$ from 78 to 310 K. Dashed arrow lines are guides to the eye on peak 1 and peak 2. (b) Excitation-power-dependent PL spectra of $(AMP)PbI_4$ at 78 K. The peak positions of peak 1 and peak 2 are 523.2 and 528.6 nm, respectively. (c) Integrated PL intensity versus excitation power of peaks 1 and 2 at 78 K. The solid lines are fitting results by a power-law function. (d) Temperature-dependent energy difference between peaks 1 and 2. (e) Temperature-dependent PL fwhm of peaks 1 and 2. The solid lines are the fitting results based on eq 3, while the dashed lines represent the acoustic-phonon coupling term $(\Gamma_{inh} + \gamma_{ac}T)$.

energy PL emission (peak 2) of $(AMP)PbI_4$ is likely to originate from the momentum-indirect exciton transition. This is further confirmed by the analysis of PL spectral weight (the integrated PL intensity of peak 2 divided by the total PL) as the function of temperature (Figure S10). From 150 K onward, the spectral weight of peak 2 begins to increase due to the increase of LO-phonon population, similar to that of the indirect PL emission in $(PEA)_2PbI_4$.[10] The time-resolved PL (TRPL) of the two different peaks at 70 K is shown in Figure S11. The slightly longer lifetime of peak 2 at 70 K can be attributed to the inefficiency of indirect transition. The relatively low P value of peak 2 (Figure 2b) can be ascribed to longer relaxation path in the indirect transition. Despite hot carrier relaxation that occurs for both direct and indirect transition, indirect excitons need to return back to Γ point via phonon scattering before radiative recombination. Besides, the relatively lower transition rate of peak 2 compared to that of spin flip might further decrease P.[30]

The excitation-power-dependent PL spectra at 78 K (Figure 3b) reveal that the dual emission peaks remain at the same position as excitation power (I_{ex}) increases. The integrated PL intensity (I_{PL}) of both peaks versus I_{ex} can be well fitted by a power-law function $I_{PL} \sim I_{ex}^k$ with the fitting parameter k of 0.985 for free exciton emission peak and 1.267 for low-energy emission peak, respectively (Figure 3c). The linear power dependence of peak 1 confirms its origin as free exciton emission,[43] while the slightly superlinear power dependence of peak 2 can exclude defect-related emission.[32] There are various mechanisms that could lead to the observed nonlinear behavior. The instability of momentum-indirect excitons might lead to the generation of free carriers in addition to excitons, resulting in a nonlinear excitonic emission under nonresonant optical pumping.[43] In addition, the carrier injection from high-energy to low-energy indirect valleys[44] might also affect the k value. Nevertheless, future experimental efforts are required to unambiguously clarify this, which are beyond the scope of the present work. Furthermore, it should be noted that other physical mechanism ranging from self-trapped excitons,[42] biexcitons,[31] polaronic effect,[33] trions,[34] phonon replicas,[35] fine-structure splitting,[36] and interplane excitons[41] can result in a low-energy PL emission. However, none of these viewpoints can satisfactorily account for the spectral characteristics of peak 2 in $(AMP)PbI_4$ (see Supporting Information for detailed analysis). Therefore, the indirect exciton transition could be the most reasonable origin of peak 2.

Since the energy difference of these two peaks (ΔE) represents the Rashba splitting energy, we are able to quantitatively investigate how Rashba splitting evolves with temperature, revealing the underlying mechanism of the thermally assisted Rashba effect in $(AMP)PbI_4$. Figure 3d displays the temperature-dependent Rashba splitting energy. ΔE remains nearly constant at low temperatures and increases monotonously with the increase of temperature from 150 K onward. This could be attributed to thermally assisted structural distortion associated with specific phonon modes.[29,30] The longitudinal optical (LO) phonon in perovskites typically corresponds to Pb−I bending or stretching,[45] which can introduce extra asymmetry via local polar fluctuation[29] and also influence SOC.[46] Since the phonon occupation number increases with temperature, thermal distortion of PbI_6 octahedra can yield a temperature-dependent Rashba splitting. In this scenario, Rashba splitting energy can be expressed as[30]

$$\Delta E = \Delta E_0 + \frac{A}{\left[\exp\left(\frac{E_{ph}}{k_B T}\right) - 1\right]} \quad (2)$$

where ΔE_0 denotes the temperature-independent term (static Rashba splitting), A is the scaling factor, k_B is the Boltzmann constant, and E_{ph} is the energy of the LO-phonon that leads to the temperature-dependent Rashba splitting term. Our measured data (ΔE) can be well fitted via eq 2 (Figure 2b), which further verifies our hypothesis. The static Rashba term ΔE_0 is fitted to be ∼21 meV. The fitted results of E_{ph} range from 65 to 75 meV, agreeing well with the peak energy of 69

https://doi.org/10.1021/acs.nanolett.1c00364
Nano Lett. 2021, 21, 4584−4591

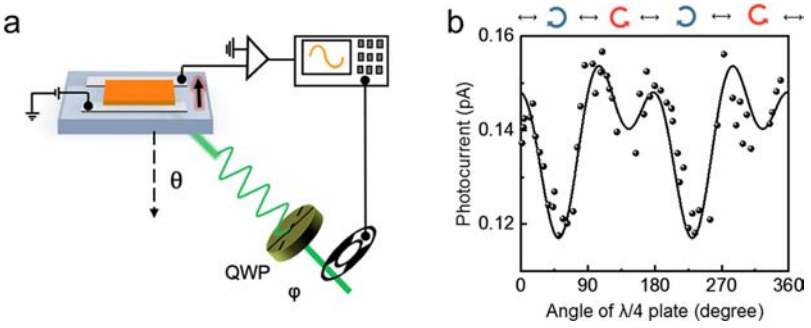

Figure 4. Photogalvanic (PGE) current in $(AMP)PbI_4$. (a) Schematic illustration of the experimental setup. The φ indicates the angle between the fast axis of the quarter-wave plate (QWP) and the incident light polarization. The θ indicates the incident angle of excitation light. (b) Room temperature photogalvanic current versus $\lambda/4$ plate rotation angle φ, measured at $\theta = 60°$, excited via a 556 nm continuous laser. The black solid line is the fit to the measured data using eq 4.

meV in the Raman spectrum (Figure S12). Furthermore, a broad background signal can be observed in the low-wavenumber range in Raman spectra (Figure S13), which is interpreted as quasi-elastic scattering caused by polar fluctuations that associated with LO phonons in perovskites, similar to the 3D perovskite cases.[37] Moreover, the broad low-wavenumber signal increases with temperature (Figure S13), which directly supports our thermally assisted Rashba splitting model because extra-symmetry breaks can be introduced via such dynamical polar fluctuations.[29,30]

Through assessing the thermal broadening of PL emission caused by electron−phonon coupling,[47,48] we can study how different phonon modes evolve with temperature in $(AMP)PbI_4$. We have extracted the full-width at half-maximum (fwhm) from PL spectra for both peaks 1 and 2 (Figure 3e). The temperature dependence of fwhm could be approximately expressed as[48]

$$\mathrm{fwhm}(T) = \Gamma_{\mathrm{inh}} + \gamma_{\mathrm{ac}} T + \frac{\gamma_{\mathrm{LO}}}{\left[\exp\left(\frac{\hbar w_{\mathrm{LO}}}{k_{\mathrm{B}} T}\right) - 1\right]} \quad (3)$$

where Γ_{inh}, γ_{ac}, γ_{LO}, and $\hbar w_{\mathrm{LO}}$ are the intrinsic fwhm, the acoustic-phonon coupling term, the LO-phonon coupling term, and the energy of the LO-phonon. As shown in Figure 3e, the solid lines are the fitting results based on eq 3, and the dashed lines denote the acoustic−phonon coupling term ($\Gamma_{\mathrm{inh}} + \gamma_{\mathrm{ac}} T$). The larger broadening of peak 2 indicates the enhanced phonon coupling and carrier scattering in these indirect bandgap valleys.[29] The fwhm versus temperature transits from linear ($\Gamma_{\mathrm{inh}} + \gamma_{\mathrm{ac}} T$) to nonlinear increase around 150 K, indicating that acoustic phonons significantly contribute to the PL broadening below 150 K while LO phonons start to play the dominant role in peak broadening at higher temperatures. This coincides with the increase of spectral weight of peak 2 from 150 K, further confirming that the rapid increase of ΔE from 150 K onward is associated with LO phonons.

To further validate the existence of Rashba splitting, we have carried out the circular photogalvanic effect (CPGE) current measurement. CPGE is regarded as an important phenomenon to verify the existence of Rashba splitting.[8,23,24,40] When Rashba splitting is present, σ^+ and σ^- polarized light will result in non-equilibrium spin polarization among the two Rashba branches,[23] resulting in the photocurrent that is sensitive to the helicity of incident light. Figure 4a illustrates our experimental setup for the helicity-dependent photocurrent measurement. A two-probe photoconductor based on the $(AMP)PbI_4$ flake was illuminated with a 556 nm (corresponding to the wavelength of peak 2) circularly polarized continuous laser beam. The polarization state of the light was modulated from σ^+ polarization to linear polarization (LP), to σ^- polarization by rotating a quarter-wave plate (QWP). The near-resonant excitation with the indirect excitons was selected for CPGE measurement. As reported in different HOIPs with Rashba splitting,[8] large spin-current can only be generated under near-resonant excitation with the indirect bandgap. The photo-generated carriers accumulated at the bottom of an indirect parabola will quickly undergo thermalization by interacting with phonons.[10] With this thermalization process, a nonzero group velocity as well as the CPGE current are yielded simultaneously.

Figure 4b shows the photoresponse under 556 nm laser excitation at zero bias with an incident angle of 60°. As can be clearly seen, the photocurrent varies periodically with the polarization of incident light. In addition, the CPGE current strongly relies on the excitation wavelength. Under off-resonant excitation with peak 2, CPGE current becomes negligible (Figure S14), similar to the 3D perovskite case.[8] This indicates that peak 2 indeed originates from Rashba splitting bands. The experimental data can be well fitted via the function[8]

$$I = C \sin(2\varphi) + L \sin(4\varphi + \theta) + D \quad (4)$$

The first term accounts for the CPGE current, the second term describes the photocurrent induced by linearly polarized light through linear photogalvanic effect (LPGE) or photon drag, and the polarization-independent component D probably originates from photovoltaic effects or hot electron injection.[49] C and L are the magnitude of CPGE current and the maginitude of photocurrent induced by LPGE or photon drag, respectively. The fitting results are shown in Table S1. Furthermore, a circular polarization sensitivity ($\frac{I(\sigma^+)}{I(\sigma^-)}$) reaches up to 1.2 based on this photodetector. This offers new opportunities for valleytronic and spintronic applications, in which efficient and selective manipulation of spin and valley freedom is essential.

CONCLUSIONS

In summary, we developed an economical and efficient aqueous method for the synthesis of $(AMP)PbI_4$ single crystals and presented a systematic study of the Rashba effect. Through

https://doi.org/10.1021/acs.nanolett.1c00364
Nano Lett. 2021, 21, 4584−4591

temperature- and polarization-dependent PL studies, we revealed that the underlying mechanism of the giant Rashba splitting in $(AMP)PbI_4$. At low temperatures, the Rashba splitting mainly originates from the static Rashba effect induced by AMP cations or surface/interface effect. When the temperature increases, both the static and dynamically thermally assisted Rashba effect contribute to the overall spin-splitting, leading to the enhanced degree of circular polarization of PL at higher temperatures. The presence of CPGE at room temperature also supports the existence of Rashba splitting. Our findings reveal that the 2D DJ perovskite $(AMP)PbI_4$ would be a promising candidate for room/high-temperature spintronics and valleytronics.

■ ASSOCIATED CONTENT

Supporting Information

The Supporting Information is available free of charge at https://pubs.acs.org/doi/10.1021/acs.nanolett.1c00364.

Sample Preparations, Material Characterizations, Device Fabrication, and CPGE Measurement, Calculation of E_R via the degree of circular polarization of PL, Origins of the low energy PL emission, including figures and tables (PDF)

■ AUTHOR INFORMATION

Corresponding Author

Dehui Li − *School of Optical and Electronic Information and Wuhan National Laboratory for Optoelectronics and School of Physics, Huazhong University of Science and Technology, Wuhan 430074, China;* orcid.org/0000-0002-5945-220X; Email: dehuili@hust.edu.cn

Authors

Boxuan Zhou − *School of Optical and Electronic Information, Huazhong University of Science and Technology, Wuhan 430074, China*

Lihan Liang − *School of Optical and Electronic Information, Huazhong University of Science and Technology, Wuhan 430074, China*

Jiaqi Ma − *School of Optical and Electronic Information, Huazhong University of Science and Technology, Wuhan 430074, China*

Junze Li − *School of Optical and Electronic Information, Huazhong University of Science and Technology, Wuhan 430074, China;* orcid.org/0000-0001-8837-5349

Wancai Li − *School of Optical and Electronic Information, Huazhong University of Science and Technology, Wuhan 430074, China*

Zeyi Liu − *School of Optical and Electronic Information, Huazhong University of Science and Technology, Wuhan 430074, China*

Haolin Li − *Department of Electrical and Electronic Engineering, Southern University of Science and Technology, Shenzhen 518055, China*

Rui Chen − *Department of Electrical and Electronic Engineering, Southern University of Science and Technology, Shenzhen 518055, China;* orcid.org/0000-0002-0445-7847

Complete contact information is available at: https://pubs.acs.org/10.1021/acs.nanolett.1c00364

Author Contributions

#B.Z. and L.L. contribute equally to this work.

Notes

The authors declare no competing financial interest.

■ ACKNOWLEDGMENTS

D. L. acknowledges the support from National Basic Research Program of China (2019YFB2203104, 2018YFA0704403), NSFC (62074064), and the Innovation Fund of WNLO. We thank Hong Cheng engineer in the Analytical and Testing Center of Huazhong University of Science and Technology for the support in PL measurement and thank the Center of Micro-Fabrication of WNLO for the support in XRD measurement.

■ REFERENCES

(1) Manchon, A.; Koo, H. C.; Nitta, J.; Frolov, S. M.; Duine, R. A. New perspectives for Rashba spin-orbit coupling. *Nat. Mater.* **2015**, *14* (9), 871−882.

(2) Lesne, E.; Fu, Y.; Oyarzun, S.; Rojas-Sánchez, J. C.; Vaz, D. C.; Naganuma, H.; Sicoli, G.; Attané, J. P.; Jamet, M.; Jacquet, E.; George, J. M.; Barthélémy, A.; Jaffrès, H.; Fert, A.; Bibes, M.; Vila, L. Highly efficient and tunable spin-to-charge conversion through Rashba coupling at oxide interfaces. *Nat. Mater.* **2016**, *15* (12), 1261−1266.

(3) Otani, Y.; Shiraishi, M.; Oiwa, A.; Saitoh, E.; Murakami, S. Spin conversion on the nanoscale. *Nat. Phys.* **2017**, *13* (9), 829−832.

(4) Koo, H. C.; Kim, S. B.; Kim, H.; Park, T. E.; Choi, J. W.; Kim, K. W.; Go, G.; Oh, J. H.; Lee, D. K.; Park, E. S.; Hong, I. S.; Lee, K. J. Rashba Effect in Functional Spintronic Devices. *Adv. Mater.* **2020**, *32* (51), 2002117.

(5) Nitta, J.; Akazaki, T.; Takayanagi, H.; Enoki, T. Gate Control of Spin-Orbit Interaction in an Inverted $In_{0.53}Ga_{0.47}As/In_{0.52}Al_{0.48}As$ Heterostructure. *Phys. Rev. Lett.* **1997**, *78* (7), 1335−1338.

(6) King, P. D.; Hatch, R. C.; Bianchi, M.; Ovsyannikov, R.; Lupulescu, C.; Landolt, G.; Slomski, B.; Dil, J. H.; Guan, D.; Mi, J. L.; Rienks, E. D.; Fink, J.; Lindblad, A.; Svensson, S.; Bao, S.; Balakrishnan, G.; Iversen, B. B.; Osterwalder, J.; Eberhardt, W.; Baumberger, F.; Hofmann, P. Large Tunable Rashba Spin Splitting of a Two-Dimensional Electron Gas in Bi_2Se_3. *Phys. Rev. Lett.* **2011**, *107* (9), 096802.

(7) Lin, W.; Li, L.; Doğan, F.; Li, C.; Rotella, H.; Yu, X.; Zhang, B.; Li, Y.; Lew, W. S.; Wang, S.; Prellier, W.; Pennycook, S. J.; Chen, J.; Zhong, Z.; Manchon, A.; Wu, T. Interface-based tuning of Rashba spin-orbit interaction in asymmetric oxide heterostructures with 3d electrons. *Nat. Commun.* **2019**, *10*, 3052.

(8) Niesner, D.; Hauck, M.; Shrestha, S.; Levchuk, I.; Matt, G. J.; Osvet, A.; Batentschuk, M.; Brabec, C.; Weber, H. B.; Fauster, T. Structural Fluctuations Cause Spin-Split States in Tetragonal $CH_3NH_3PbI_3$ as Evidenced by the Circular Photogalvanic Effect. *Proc. Natl. Acad. Sci. U. S. A.* **2018**, *115* (38), 9509−9514.

(9) Ye, Y.; Ye, Z.; Gharghi, M.; Zhu, H.; Zhao, M.; Yin, X.; Zhang, X. Distinguishing between dynamical and static Rashba effects in hybrid perovskite nanocrystals using transient absorption spectroscopy. *arXiv*, 2019, 1305.4235. http://arxiv.org/abs/1305.4235 (accessed June 2014).

(10) Do, T. T. H.; Granados del Águila, A.; Xing, J.; Liu, S.; Xiong, Q. Direct and indirect exciton transitions in two-dimensional lead halide perovskite semiconductors. *J. Chem. Phys.* **2020**, *153* (6), 064705.

(11) Chen, Y.; Sun, Y.; Peng, J.; Zhang, W.; Su, X.; Zheng, K.; Pullerits, T.; Liang, Z. Tailoring Organic Cation of 2D Air-Stable Organometal Halide Perovskites for Highly Efficient Planar Solar Cells. *Adv. Energy Materials* **2017**, *7* (18), 1700162.

(12) Park, B. W.; Seok, S. I. Intrinsic Instability of Inorganic-Organic Hybrid Halide Perovskite Materials. *Adv. Mater.* **2019**, *31* (20), 1805337.

(13) Martiradonna, L. Riddles in Perovskite Research. *Nat. Mater.* **2018**, *17* (5), 377−379.
(14) Xiao, Z.; Meng, W.; Wang, J.; Mitzi, D. B.; Yan, Y. Searching for Promising New Perovskite-Based Photovoltaic Absorbers: the Importance of Electronic Dimensionality. *Mater. Horiz.* **2017**, *4* (2), 206−216.
(15) Yusoff, A. R. b. M.; Nazeeruddin, M. K. Low-Dimensional Perovskites: From Synthesis to Stability in Perovskite Solar Cells. *Adv. Energy Mater.* **2018**, *8* (26), 1702073.
(16) Zhai, Y.; Baniya, S.; Zhang, C.; Li, J.; Haney, P.; Sheng, C. X.; Ehrenfreund, E.; Vardeny, Z. V. Giant Rashba splitting in 2D organic-inorganic halide perovskites measured by transient spectroscopies. *Sci. Adv.* **2017**, *3* (7), e1700704.
(17) Park, I. H.; Zhang, Q.; Kwon, K. C.; Zhu, Z.; Yu, W.; Leng, K.; Giovanni, D.; Choi, H. S.; Abdelwahab, I.; Xu, Q.-H.; Loh, K. P. Ferroelectricity and Rashba Effect in a Two-Dimensional Dion-Jacobson Hybrid Organic-Inorganic Perovskite. *J. Am. Chem. Soc.* **2019**, *141* (40), 15972−15976.
(18) Ahmad, S.; Fu, P.; Yu, S.; Yang, Q.; Liu, X.; Wang, X.; Wang, X.; Guo, X.; Li, C. Dion-Jacobson Phase 2D Layered Perovskites for Solar Cells with Ultrahigh Stability. *Joule* **2019**, *3* (3), 794−806.
(19) Park, I. H.; Kwon, K. C.; Zhu, Z.; Wu, X.; Li, R.; Xu, Q. H.; Loh, K. P. Self-Powered Photodetector Using Two-Dimensional Ferroelectric Dion−Jacobson Hybrid Perovskites. *J. Am. Chem. Soc.* **2020**, *142* (43), 18592−18598.
(20) Fang, Z.; Shang, M.; Zheng, Y.; Du, Z.; Wang, G.; Duan, X.; Chou, K. C.; Lin, C. H.; Yang, W.; Hou, X.; Wu, T. Organic intercalation engineering of quasi-2D Dion-Jacobson α-$CsPbI_3$ perovskites. *Mater. Horiz.* **2020**, *7* (4), 1042−1050.
(21) Picozzi, S. Ferroelectric Rashba semiconductors as a novel class of multifunctional materials. *Front. Phys.* **2014**, *2*, 10.
(22) Mao, L.; Ke, W.; Pedesseau, L.; Wu, Y.; Katan, C.; Even, J.; Wasielewski, M. R.; Stoumpos, C. C.; Kanatzidis, M. G. Hybrid Dion−Jacobson 2D Lead Iodide Perovskites. *J. Am. Chem. Soc.* **2018**, *140* (10), 3775−3783.
(23) Liu, X.; Chanana, A.; Huynh, U.; Xue, F.; Haney, P.; Blair, S.; Jiang, X.; Vardeny, Z. V. Circular photogalvanic spectroscopy of Rashba splitting in 2D hybrid organic−inorganic perovskite multiple quantum wells. *Nat. Commun.* **2020**, *11*, 323.
(24) Yuan, H.; Wang, X.; Lian, B.; Zhang, H.; Fang, X.; Shen, B.; Xu, G.; Xu, Y.; Zhang, S. C.; Hwang, H. Y.; Cui, Y. Generation and electric control of spin−valleycoupled circular photogalvanic current in WSe_2. *Nat. Nanotechnol.* **2014**, *9* (10), 851−857.
(25) Zeng, H.; Dai, J.; Yao, W.; Xiao, D.; Cui, X. Valley polarization in MoS_2 monolayers by optical pumping. *Nat. Nanotechnol.* **2012**, *7* (8), 490−493.
(26) Kioseoglou, G.; Hanbicki, A. T.; Currie, M.; Friedman, A. L.; Jonker, B. T. Optical polarization and intervalley scattering in single layers of MoS_2 and $MoSe_2$. *Sci. Rep.* **2016**, *6*, 25041.
(27) Wang, J.; Fang, C.; Ma, J.; Wang, S.; Jin, L.; Li, W.; Li, D. Aqueous Synthesis of Low-Dimensional Lead Halide Perovskites for Room-Temperature Circularly Polarized Light Emission and Detection. *ACS Nano* **2019**, *13* (8), 9473−9481.
(28) Wang, T.; Daiber, B.; Frost, J. M.; Mann, S. A.; Garnett, E. C.; Walsh, A.; Ehrler, B. Indirect to direct bandgap transition in methylammonium lead halide perovskite. *Energy Environ. Sci.* **2017**, *10* (2), 509−515.
(29) Steele, J. A.; Puech, P.; Monserrat, B.; Wu, B.; Yang, R. X.; Kirchartz, T.; Yuan, H.; Fleury, G.; Giovanni, D.; Fron, E.; Keshavarz, M.; Debroye, E.; Zhou, G.; Sum, T. C.; Walsh, A.; Hofkens, J.; Roeffaers, M. B. J. Role of Electron-Phonon Coupling in the Thermal Evolution of Bulk Rashba-Like Spin Split Lead Halide Perovskites Exhibiting Dual Band Photoluminescence. *ACS Energy Lett.* **2019**, *4* (9), 2205−2212.
(30) Wu, B.; Yuan, H.; Xu, Q.; Steele, J. A.; Giovanni, D.; Puech, P.; Fu, J.; Ng, Y. F.; Jamaludin, N. F.; Solanki, A.; Mhaisalkar, S.; Mathews, N.; Roeffaers, M. B. J.; Grätzel, M.; Hofkens, J.; Sum, T. C. Indirect tail states formation by thermal-induced polar fluctuations in halide perovskites. *Nat. Commun.* **2019**, *10*, 484.
(31) Thouin, F.; Neutzner, S.; Cortecchia, D.; Dragomir, V. A.; Soci, C.; Salim, T.; Lam, Y. M.; Leonelli, R.; Petrozza, A.; Kandada, A. R. S.; Silva, C. Stable biexcitons in two-dimensional metal-halide perovskites with strong dynamic lattice disorder. *Phys. Rev. Mater.* **2018**, *2* (3), 034001.
(32) Fang, X.; Zhang, K.; Li, Y.; Yao, L.; Zhang, Y.; Wang, Y.; Zhai, W.; Tao, L.; Du, H.; Ran, G. Effect of excess $PbBr_2$ on photoluminescence spectra of $CH_3NH_3PbBr_3$ perovskite particles at room temperature. *Appl. Phys. Lett.* **2016**, *108* (7), 071109.
(33) Itoh, T.; Nishijima, M.; Ekimov, A. I.; Gourdon, C.; Efros, A. L.; Rosen, M. Polaron and Exciton-Phonon Complexes in CuCl Nanocrystals. *Phys. Rev. Lett.* **1995**, *74* (9), 1645−1648.
(34) Plechinger, G.; Nagler, P.; Kraus, J.; Paradiso, N.; Strunk, C.; Schuller, C.; Korn, T. Identification of excitons, trions and biexcitons in single-layer WS_2. *Phys. Status Solidi RRL* **2015**, *9* (8), 457−461.
(35) Myagkota, S. V.; Gloskovskii, A. V.; Voloshinovskii, A. S. Photo- and X-ray luminescence spectra of $CsPbX_3$ microcrystals dispersed in a PbX_2 (X = Cl, Br) matrix. S. *Opt. Spectrosc.* **2000**, *88* (4), 538−541.
(36) Do, T. T. H.; Granados del Águila, A.; Zhang, D.; Xing, J.; Liu, S.; Prosnikov, M. A.; Gao, W.; Chang, K.; Christianen, P. C. M.; Xiong, Q. Bright Exciton Fine-Structure in Two-Dimensional Lead Halide Perovskites. *Nano Lett.* **2020**, *20*, 5141−5148.
(37) Yaffe, O.; Guo, Y. S.; Tan, L. Z.; Egger, D. A.; Hull, T.; Stoumpos, C. C.; Zheng, F.; Heinz, T. F.; Kronik, L.; Kanatzidis, M. G.; Owen, J. S.; Rappe, A. M.; Pimenta, M. A.; Brus, L. E. Local Polar Fluctuations in Lead Halide Perovskite Crystals. *Phys. Rev. Lett.* **2017**, *118* (13), 136001.
(38) Myung, C. W.; Javaid, S.; Kim, K. S.; Lee, G. Rashba-Dresselhaus Effect in Inorganic/Organic Lead Iodide Perovskite Interfaces. *ACS Energy Lett.* **2018**, *3* (6), 1294−1300.
(39) Ma, J.; Fang, C.; Chen, C.; Jin, L.; Wang, J.; Wang, S.; Tang, J.; Li, D. Chiral 2D Perovskites with a High Degree of Circularly Polarized Photoluminescence. *ACS Nano* **2019**, *13* (3), 3659−3665.
(40) Martiradonna, L. The influence of the Rashba effect. *Nat. Mater.* **2018**, *17* (5), 377.
(41) Wang, M.; Tang, J.; Wang, H.; Zhang, C.; Zhao, Y. S.; Yao, J. Grain Boundary Enhanced Photoluminescence Anisotropy in Two-Dimensional Hybrid Perovskite Films. *Adv. Opt. Mater.* **2020**, *8* (7), 1901780.
(42) Yu, J.; Kong, J.; Hao, W.; Guo, X.; He, H.; Leow, W. R.; Liu, Z.; Cai, P.; Qian, G.; Li, S.; Chen, X.; Chen, X. Broadband Extrinsic Self-Trapped Exciton Emission in Sn-Doped 2D Lead-Halide Perovskites. *Adv. Mater.* **2018**, *31* (7), 1806385.
(43) Schmidt, T.; Lischka, K. Excitation-power dependence of the near-band-edge photoluminescence of semiconductors. *Phys. Rev. B: Condens. Matter Mater. Phys.* **1992**, *45* (16), 8989−8994.
(44) Chen, Y.; Wang, T.; Li, Z.; Li, H.; Ye, T.; Wetzel, C.; Li, H.; Shi, S. F. Communicating Two States in Perovskite Revealed by Time-Resolved Photoluminescence Spectroscopy. *Sci. Rep.* **2018**, *8*, 16482.
(45) Wright, A. D.; Verdi, C.; Milot, R. L.; Eperon, G. E.; Herz, L. M. Electron−phonon coupling in hybrid lead halide perovskites. *Nat. Commun.* **2016**, *7*, 11755.
(46) Amat, A.; Mosconi, E.; Ronca, E.; Quarti, C.; Umari, P.; Nazeeruddin, M. K.; Grätzel, M.; Angelis, F. D. Cation-Induced Band-Gap Tuning in Organohalide Perovskites: Interplay of Spin-Orbit Coupling and Octahedra Tilting. *Nano Lett.* **2014**, *14* (6), 3608−3616.
(47) Viswanath, A. K.; Lee, J. I.; Kim, D.; Lee, C. R.; Leem, J. Y. Exciton-phonon interactions, exciton binding energy, and their importance in the realization of room-temperature semiconductor lasers based on GaN. *Phys. Rev. B: Condens. Matter Mater. Phys.* **1998**, *58*, 16333−16339.
(48) Chen, R.; Li, D.; Liu, B.; Peng, Z.; Gurzadyan, G. G.; Xiong, Q.; Sun, H. Optical and Excitonic Properties of Crystalline ZnS Nanowires: Toward Efficient Ultraviolet Emission at Room Temperature. *Nano Lett.* **2010**, *10* (12), 4956−4961.

https://doi.org/10.1021/acs.nanolett.1c00364
Nano Lett. 2021, 21, 4584−4591

(49) Ji, Z.; Liu, G.; Addison, Z.; Liu, W.; Yu, P.; Gao, H.; Liu, Z.; Rappe, A. M.; Kane, C. L.; Mele, E. J.; Agarwal, R. Spatially dispersive circular photogalvanic effect in a Weyl semimetal. *Nat. Mater.* **2019**, *18* (9), 955−962.

https://doi.org/10.1021/acs.nanolett.1c00364
Nano Lett. 2021, 21, 4584−4591